Active Remote Sensing for Saline Soils Mapping in Arid and Semi-Arid Environments

Abdelgadir Abuelgasim[1] , Muhagir El Kamali[2], Alya Aldhaheri[2]
[1]Rabdan Academy, 65 Alinshirah Street, Alsa'adah, Abu Dhabi, 22401, United Arab Emirates, aabuelgasim@ra.ac.ae

[2]Department of Geography and Urban Sustainability, College of Humanities and Social Sciences,
United Arab Emirates University, Al Ain, 15551, UAE

Abstract

Mapping of human induced or natural occurring saline soils using satellite remote sensing has been an active area of research in the past few decades. In particular in agricultural lands as saline soils negatively impact crop yield and plant growth. Within arid and semi-arid regions saline soils have adverse effects on urban structures, land surface subsidence, soil erosion and soil degradation. While most previous studies of mapping saline soils have focused on broad-band passive remote sensing data, there has been minimal exploration into the utilization of active radar remote sensing data, particularly Synthetic Aperture Radar (SAR). This research aims to bridge this gap by employing C-band Sentinel-1 data enhanced by the polarimetric analysis, to identify and map saline soils within arid and semi- arid environments. Preliminary results highlight the challenges of using active remote sensing in mapping saline soils. Relying on the correlations between electric conductivity measurements and with scattering entropy resulted in accuracies of only 17% and 15% using polarimetric anisotropy. Other soil parameters such as soil electric properties, and perhaps soil moisture would improve the detection of saline soils using SAR data. However, the incorporation of polarimetric SAR (PolSAR) techniques offers a new avenue for improving soil salinity mapping by leveraging the unique scattering mechanisms and dielectric properties of saline soils.

Keywords: Soil Salinity, Synthetic Aperture Radar, Arid, Semi-Arid, Sabkha

1. Introduction

Remote sensing of saline soils has been an active area of research in the past few decades. This is particularly so as soil salinity is a major geo-hazard in both agricultural lands and arid and semi-arid regions. Saline soil adversely affect soil and play a major role in soil erosion, dispersion and degradation (Youssef et al., 2012). Furthermore, saline soils in arid and semi-arid regions lead, in certain situations, to land subsidence, and ground upheaval (Abuelgasim and Ammad, 2019). In agricultural lands saline soils lead to reduced agricultural productivity, interference with plant nutrition and soil erosion.

Mapping saline soils is carried out using various techniques and procedures ranging from direct field observations and sampling to space based remote sensing techniques. Remote sensing provides a less costly procedure due to the large global spatial coverage, continuous repetitive coverage and high quality earth observations (Ivushkin et al., 2019; Abuelgasim and Ammad, 2019; Ma et al., 2021). Most of the remote sensing of saline soils have focused on the passive remote sensing part with primary focus on the spectral ranges in the near infra-red and the short-wave infra-red. However, the application of Synthetic Aperture Radar (SAR) in soil salinity mapping remains widely underexplored. SAR satellites illuminate ground targets with radar signals and analyze the returned backscatter, which contains crucial information about the ground surface, including soil moisture and salinity levels. Polarimetric SAR (PolSAR) extends this by analyzing the returned signal in multiple polarization states, offering insights into the surface's scattering mechanisms and enhancing soil salinity detection whether for agricultural lands or arid and semi-arid regions.

The complexity of saline soil signatures, particularly in arid and semi-arid environments, presents challenges for remote sensing. The interaction between saline soils and radar backscatter is influenced by various factors, including the soil's dielectric constant, which is directly related to its salinity and moisture content. This research aims to address these challenges by integrating PolSAR techniques with traditional SAR analysis, providing a more nuanced understanding of saline soil characteristics and improving mapping accuracy.

Most of the studies that used SAR data for mapping saline soils attempted to develop empirical regression models between the backscattered SAR signal and soil salinity. For example, Barbouchi et al. (2015) constructed a regression model to monitor Electrical Conductivity (EC) variation from interferometric coherence using Radarsat-2 (C-band) Quad Pol. This model was tested over two sites located in a semi-arid region, the first in Tunisia and the second in Morocco. The best regression model found was HH polarization with a coefficient of determination (R2) of 0.36. Gao et al. (2021) generated a linear regression model by utilizing quad polarization SAR data from Gaofen-3 (C-band) and ALOS-2 (L-band) over the arid climate of Qinghai, China. The regression model included backscattering coefficient of VV polarization, co-polarization ratio (σ_HH/σ_VV), and scattering entropy H with a determination coefficient of 0.79.

Other studies used supervised learning models such as Nurmemet et al. (2018) that utilized the Support Vector Machine (SVM) with the PALSAR-2 (L-band) Quad Pol over the arid climate of Keriya Oasis, China. Polarimetric decomposition features were the explanatory variables to the SVM with the Wrapper Feature Selector (WFS) to optimize the variables for the SVM and showed an overall accuracy of 87.57%. Taghadosi et al. (2018) performed the same technique

but by using the textural features of the Sentinel-1 (C-band) data over a hot dry climate of Kuh Sefid, Iran. Textural features of SAR data from the Grey Level Co-occurrence Matrix were optimized using the feature selection techniques and the SVR applied with different kernel functions. The best model was found with the Genetic Algorithm feature selection technique and the Radial Basis Function kernel by a coefficient of determination (R2) of 0.97.

Some studies used machine learning techniques such as Jiang et al. (2018) investigated the soil salinity by performing the machine learning techniques of Support Vector Machine (SVM) and Artificial Neural Network (ANN) with multi-source remote sensing data over Yanqi Basin, China. Variables that were employed to model the soil salinity were the backscattering coefficient from Sentinel-1, groundwater depth and soil index from Landsat 8, and surface evapotranspiration from MODIS. The SVM showed better prediction for soil salinity than ANN with a determination coefficient of 0.82 and 0.79, respectively. Hoa et al. (2019) performed the same technique with the same SAR data over the tropical climate of the agricultural regime in the Mekong River Delta, Vietnam. The extracted textural features were processed by multiple machine learning techniques and Gaussian Processes showed the best prediction of soil salinity with a correlation coefficient of 0.8 between the observed and the modeled salinity.

Periasamy and Ravi (2020) built a semi-empirical dielectric model using Sentinel-1 SAR data soil field data to quantify the backscattering coefficient over bare soil and vegetated soil in Vellore, Tamil Nada, India. The model was constructed based on the three-dimensional density space between sigma naught of VV polarization, soil texture, and in-situ dielectric constant. This model relies on the saturation state of the soil, which is constructed upon the semi-saturated state and showed a good prediction of dielectric constant in saline soil and non-saline soil with a determination coefficient of 0.8.

The primary objectives of this study are to assess the feasibility of using active remote sensing in mapping and accurately identifying saline soils in arid open desert surfaces. While this study adds to the limited literature in using SAR data for saline soils mapping, it attempts to improve the accuracy of detection with special focus on arid and semi-arid environments. This reduces the complexity of saline soils detection that might be encountered in vegetated plantations. The study aims to address these challenges by integrating PolSAR techniques with traditional SAR analysis, providing a more nuanced understanding of saline soil characteristics and improving mapping accuracy.

2. Study Area

The United Arab Emirates (UAE) is located in the south eastern part of the Arabian Peninsula at 22° 50′–26° 4′ N latitude and 51° 5′–56° 25′ E longitude (Figure 1). It is a union of 7 emirates with the emirate of Abu Dhabi being the largest in terms of land size and population. It is relatively small country with an approximate total area of 83,600 km2 dominant by massive desert landscape. In spite of its relatively small size, it has diverse ecosystems such coastal areas with vast tracks of coastal mangrove forests, mountainous regions in the northern and eastern parts and dominant fields of sand dunes.

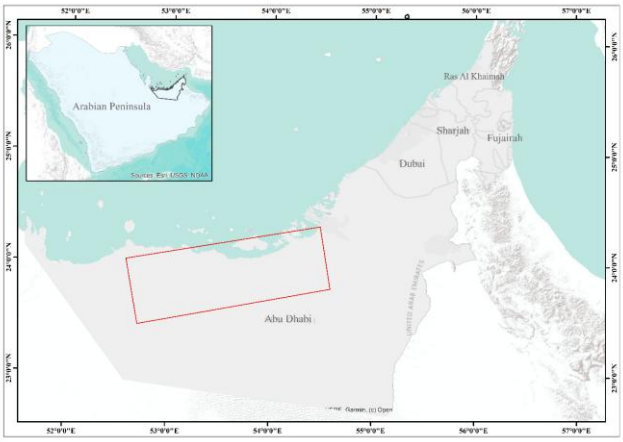

Figure 1: Study Area

The study area is located in the western side of the emirate of Abu Dhabi. It is located between 24° 07′ N 52° 42′ E and 23° 30′ N 54° 06 E′. The study area is about 7960 km2 a predominant desert surface with massive sand dune fields, it also has endangered animal conservation areas, scattered vegetation and palm tree plantations. Small towns and villages are within the study area along with the oil and gas fields. This particular area has vast large areas of saline soils including both coastal and inland sabkhas. The word “sabkha” is an Arabic description for a salt flat (Figure 2). Sabkhas are geologic features characterized by salt marshes and salt flats which are typically found in arid and semi-arid climatic conditions, in shallow continental shelf/marine environment (Evans et al., 1969). Sabkhas pose a serious geotechnical threat as they are likely to, initiate cracks in surfaces because of uneven dehydration of gypsum, compromise soil strength, corrode steel due to presence of highly concentrated sulphate and carbonate salts and lastly, crumble concrete owing to the crystallization pressure which built up as a response to evaporation of water (Youssef et al., 2012).

Figure 2: Sabkha within the study area

The UAE falls among the most driest and hottest places on earth (Abuelgasim and Ammad, 2019). The climate of the UAE is extremely arid with very dry hot and humid summers and sporadic rain falls in the winter. The average annual precipitation is just below 120 mm. These climatic conditions

make the perfect environment for salt flats development. The extremely high temperature with significant high evaporation rates results in the precipitation of insoluble salts in large quantities over vast open areas. Sabkhas and other saline surfaces can easily be identified visually on both satellite SAR and multi-spectral data.

3. Satellite and Field Data

3.1 SAR DATA

In this investigation, Sentinel-1 C-band Synthetic Aperture Radar (SAR) data is utilized to explore saline soil mapping in arid and semi-arid terrains. The C-band, with a frequency range of 4-8 GHz, offers specific advantages and limitations when compared to the deeper penetrating L-band SAR, which operates at 1-2 GHz. While L-band SAR is renowned for its ability to penetrate deeper into the Earth's surface, offering a more profound understanding of sub-surface features due to its longer wavelength, the Sentinel-1 C-band provides finer spatial resolution and is more sensitive to surface roughness and moisture content, factors crucial for identifying saline soils. In arid and semi-arid regions, the surface soil layer is often desiccated, making surface characteristics critical for salinity detection. The penetration depth of the radar signal is a significant factor in these environments as it can influence the detection of subsurface moisture and soil structure, which are closely linked to salinity levels. Although the L-band might offer better insights into deeper soil layers, the operational advantages of the Sentinel-1 C-band, including its frequent revisit times and broad area coverage, make it a practical choice for monitoring changes in surface salinity over time. This study aims to assess the suitability of Sentinel-1 C-band specifications for soil salinity mapping in such environments, acknowledging the trade-offs between penetration depth and the ability to capture surface salinity indicators critical for effective monitoring and management of saline soils. the dual polarization, Vertical transmit Vertical receive (VV) and Vertical transmit Horizontal receive (VH). The imaging mode of the Sentinel-1 SAR satellite is the Interferometric Wide Swath (IW) divided int three sub-swaths and nine bursts each with total swath width of 250 km and 5 m by 20 m spatial resolution in range and azimuth direction, respectively in the Single Look Complex (SLC) product level. The Sentinel-1 data was obtained over the study area along descending orbit from the European Space Agency (ESA) Copernicus open hub on November, 4th 2020 in coincidence with the field observations date.

3.2 Field Soil Samples Collection

The field sampling process was conducted within the first ten days of November 2020. It has been carried out during extremely dry weather conditions as no rainfall was reported within the study area. Areas where soil samples were to be collected were selected a priori through the visual analysis of satellite image data and topographic maps of the area. The key important criteria in selecting sampling locations were, ease of access, and avoidance of gas and oil fields as well as military installations. Sabkhas were easy identified in the multispectral and SAR image data as well as the topographic maps. Both inland sabkhas and coastal ones were included in the sampling process. Other locations were chosen due to the tonal variations of the soil color in the image data assumed to be indicative of different soil types with different levels of salinity.

Figure 3: Soil Samples Locations

In total 400 points were selected, of which 338 were used for developing statistical regression models and 62 for testing the models. Small spades were used to scarp the top surface of the soil (Sparks et al., 1996). A hand-held global position system (GPS) receiver was used to mark the location of the sample for later identification in the image data. Collected soil samples were labelled and stored in airlock plastic bags and taken for the geology lab for salinity analysis. Figure 3 shows the locations of the points sampled within the study area.

4. Methodology

4.1 Image Processing

Sentinel-1A SLC image was processed by the open-source SeNtinel Application Platform (SNAP) to retrieve backscattering coefficients for both VV and VH. The pre-processing steps involved radiometric calibration, multi-looking, and geometric and terrain corrections. Radiometric calibration was performed to calculate the radar cross section known as sigma naught which is sensitive to the incidence angle variation across the swath. However, for this study we used gamma coefficient instead, which is the sigma naught corrected for the local incidence angle. Multi-looking process in order to achieve better radiometric resolution and reduce the speckle appearance in the image. It was performed with 4 looks in range and one look in azimuth. Geometric and terrain correction was performed by applying the range-doppler terrain correction tool with a Digital Elevation Model (DEM) in order to correct the geometrical mis shift and align pixels with their correct geographical orientation.

Polarimetric decomposition (Cloude and Pottier, 1996) was utilized to extract meaningful information from the VV and VH images. The polarimetric decomposition technique used was H-α decomposition, which produces Entropy (H), Anisotropy (A), and Alpha (α) parameters. The Entropy parameter is the randomness of the scattering mechanisms occurred at the scatterer, while Anisotropy is an index represents the relative probability between secondary scattering mechanisms, and Alpha parameter represents the scattering angle which can be used to classify the scattering process (surface, double-bounce, or volume) across the image.

These parameters help in classification of SAR images based on the scattering mechanism which as above-mentioned where the

challenge of mapping soil salinity from SAR images. Understanding the relationship between these parameters and soil salinity will reduce the uncertainty level and help in developing better models for mapping soil salinity using SAR images.

4.2 Lab Analysis

The lab analysis consisted of several steps for estimating the salinity levels of the collected samples. Each sample was first air dried at lab room temperature. A geologic hammer was used to ground the samples, and the resulting mixture was sieved to insure homogeneity (Sparks et al., 1996, Kissell and Sonon, 2008). A solution in the ratio of 1:2 soil sample by mass and deionized water by volume (Sparks et al., 1996) respectively, was prepared for each sample. Through mixing was performed on the water and soil samples to insure all soluble salts are properly dissolved. The solution was later filtered in preparation for salinity measurement using and electric conductivity meter.

A widely used technique for measuring soil salinity is the employment of electrical conductivity (EC) meters (McNeill, 1992; Rhoades, 1993; Abuelgasim and Ammad, 2017; Abuelgasim and Ammad, 2019). A HACH HQ40D Portable Multi Meter was used to measure the salinity. The meter provides measures of EC in the range 0.01 µS/cm - 200.0 mS/cm and measure of parts per thousands. Only the EC measurements were used in this study.

Four hundred samples were analyzed in the lab. The resulting soil salinity measures were compared with the Soil Test Handbook for Georgia (Kissell and Sonon, 2008). This table provides a description of different soil salinity categories. Table 1.

Soil Salinity Category	**EC Measurement (dS/m)**	**Soil Characteristic**
Non-Saline	0–0.15	Very low
Slightly Saline/Low Salinity	0.15–0.50	Low
Moderately Saline/Medium Salinity	0.51–1.25	Medium
Strongly Saline/High Salinity	1.26–1.75	High
Very High Salinity	1.76–2.00	Very high
Excessively High Salinity	>2.00	Excessively high

Table 1: Soil Salinity Categories

This soil salinity classification system yields six categories ranging from non-saline soils to excessively high saline ones. It was developed with agricultural soils in mind, however. Within arid and semi-arid regions sabkha areas can have salinities exceeding 500 dS/m.

As shown in table 2 It was found that the 400 samples fell in different soil salinity classes. Table 2 also suggests that generally this particular region has high levels of soil salinity throughout the study area. The minimum measured salinity was 0.066 dS/m and the maximum was 228 dS/m.

Soil Salinity Class	**Number of Samples**
Non-Saline	22
Slightly Saline/Low Salinity	151
Moderately Saline/Medium Salinity	65
Strongly Saline/High Salinity	18
Very High Salinity	8
Excessively High Salinity	136

Table 2: Samples Soil Salinity Classes

4.3 Empirical Model Development and Statistical Regression

In remote sensing modeling the interaction between reflected electromagnetic radiation and land surface physical and biophysical parameters has been active area of research. The major objectives of such modeling processes are the development of empirical models that can be later be used to estimate or derive surface parameters from reflected data. Such approach has been widely used in estimating soil salinity from both passive and active remote sensing data (Abuelgasim and Ammad, 2019; El-Battay et al., 2017; Bannari et al., 2008; Zribi et al., 2014; Allbed et al., 2014; Kaplan, et al. 2023).

To develop empirical models for saline soils a regression analysis was conducted between the parameters derived from the Sentinel-1 data and the measured soil salinity. The derived parameters were entrophy, anisotropy, alpha, gamma0VH, gamma0VV. Various statistical regression models were explored, however. It was found that the polynomial regression technique yielded better correlation. The field samples were divided into two groups one from developing the empirical model (338 samples) and one for testing the developed model (54 samples). Some of the soil samples locations fell outside the coverage of the Sentilnel-1 coverage and were excluded from the analysis.

5. Results and Discussions

5.1 Statistical Regression

Figures 4-8 show the results of the regression analysis between the parameters derived from the Sentinel-1 data and the soil salinity measurements.

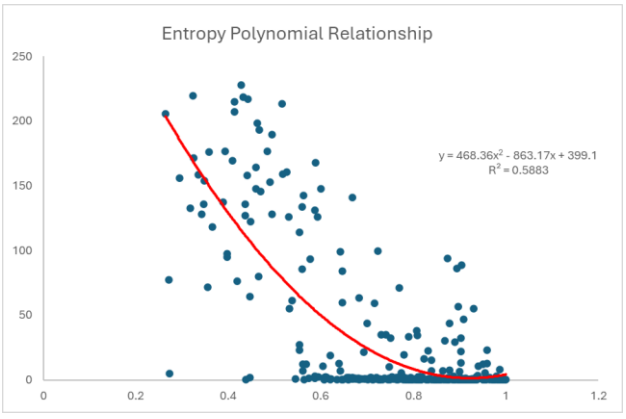

Figure 4: Entropy Soil Salinity Model

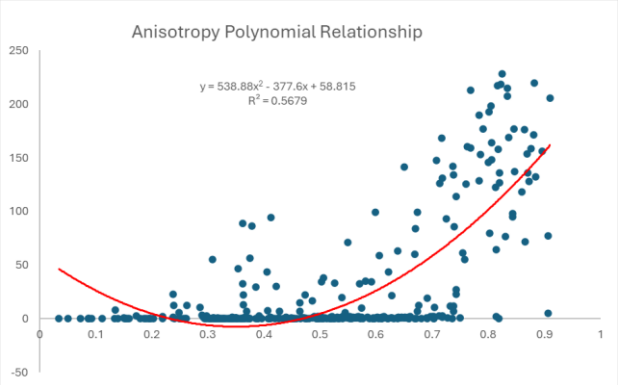

Figure 5: Anisotropy Soil Salinity Model

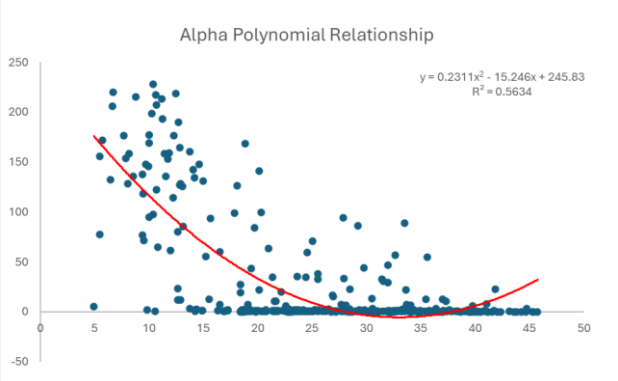

Figure 6: Alpha Soil Salinity Model

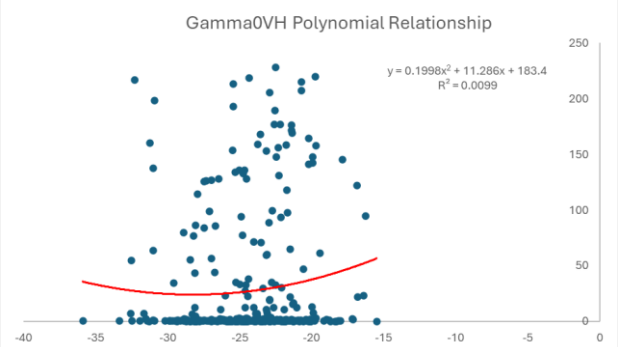

Figure 7: Gamma0VH Soil Salinity Model

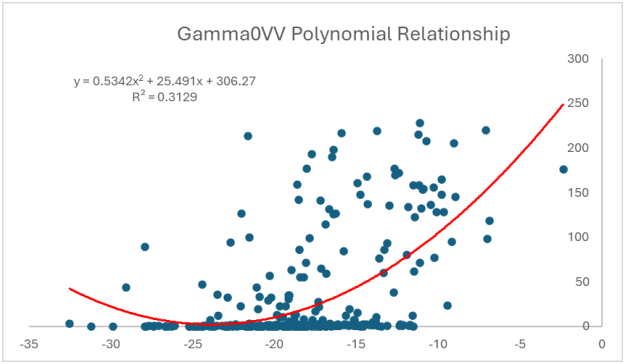

Figure 8: Gamma0VV Soil Salinity Model

As per the displayed R-square measure the results of the regression between the SAR parameters and soil salinity show variables levels of accuracy (0.01-0.59) as shown in table 3.

Parameter	R-Square	Correlation
Entropy	0.59	-0.711
Anisotropy	0.57	0.612
Alpha	0.56	-0.621
Gamma0VH	0.010	0.081
Gamma0VV	0.313	0.476

Table 3: R-Square and Correlation Results

5.2 Soil Salinity Classes

Using the developed statistical models, it will be possible to generate soil salinity model estimates for each pixel in the image's study area, however. This research uses the concept of salinity level categories map for displaying the overall salinity within the study area, instead of actual model estimations of salinity per image pixel (Abuelgasim and Ammad, 2019). This would portray better the geographic spatial distribution of soil salinity within the study area. The soil salinity class maps developed here categorize model pixel estimated salinities as per the (Kissell and Sonon, 2008) soil salinity classification. For each salinity level class, a range of salinity values as predicted by the models are associated with a particular class type ranging from non-saline soils class to excessively high salinity class as shown in table 1. Only the entropy and anisotropy maps are shown here.

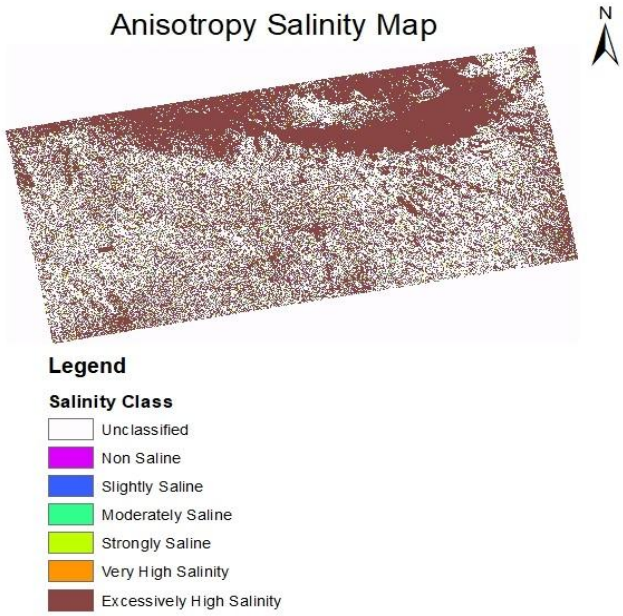

Figure 9: Anisotropy Soil Salinity Map

Salinity Class				Map				Accuracy
	Unclassified	1	2	3	4	5	6	
Unclassified	0	0	0	0	0	0	0	
Non-Saline Soils	0	0	0	0	1	0	5	0.00%
Low Salinity	0	0	0	0	5	3	24	0.00%
Medium Salinity	0	0	0	0	1	0	4	0.00%
High Salinity	0	0	0	0	0	0	1	0.00%
Very High Salinity	0	0	0	0	0	0	0	0.00%
Excessively High Salinity/Sabkha	0	0	0	0	0	0	9	100.00%
Overall accuracy								**17.00%**

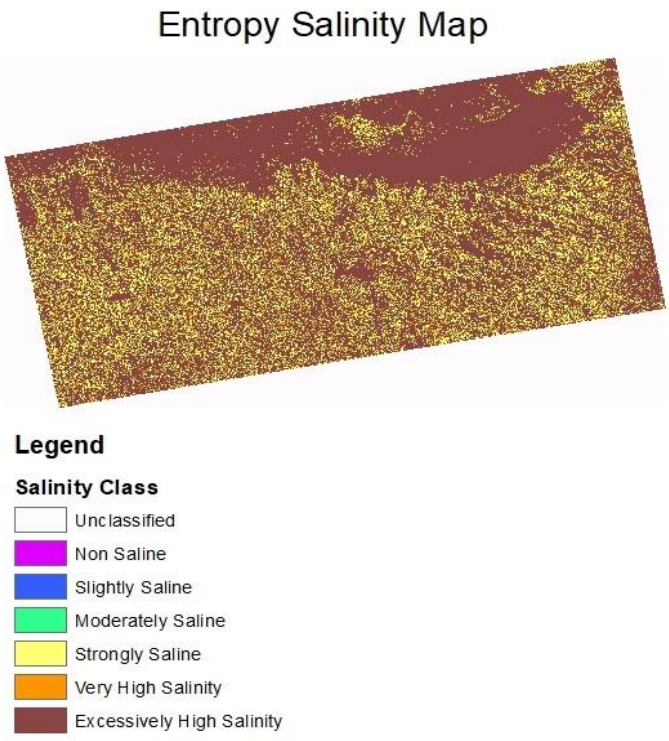

Figure 9: Entropy Soil Salinity Map

The maps above (Figure 9-10) show the predicted salinity classes within the study area. As can be noticed in the entropy classified image there is significant over estimation for the excessively saline and strongly saline areas. Almost little to no other areas with other salinity classes can be observed in the image. This is naturally not the case as previous studies using multi-spectral data within the same study area have portrayed diverse and different distribution of saline soils (Abuelgasim and Ammad, 2019).

The anisotropy classified image shows even a more erroneous pattern. More than half of the image remains unclassified. The reason is that the resulting salinity values for these areas are below zero. This is also not the case for this particular area, in addition, negative salinity levels physically do not make much reason.

5.3 Confusion Matrices

Table 4: Entropy Confusion Matrix

Tables 4 and 5 above show significant low accuracy, where entropy data shows only 17% and the anisotropy data shows 15% accuracy. This indicates that active remote sensing have significant limitations in mapping saline soils, as previous studies using broad band passive remote sensing data have yielded much higher accuracies. This is an interesting finding that can better be explained through analyzing the interaction between soil surfaces and radar signals.

Radar signal scattering from soil depends mainly on soil grain size, moisture content, and salinity content (Periasamy and Ravi, 2020). Since the sampling has been conducted during the dry period before the rainy season in the study area the effect of the moisture content will be too small. Generally, higher salinity in the soil increases the backscattering coefficient due to increasing dielectric constant in the soil. Also, higher salinity

levels in soil surfaces, generally increases the soil roughness which in turn increases the backscattering coefficient.. In the case of extremely high salinity soils, such as Sabkhas, soil surface cracks due to high dryness and forms repeated small convex layers in the wavelength scale. This special case of high salinity soil surface can be categorized as a Bragg scattering surface which shows a higher backscattering coefficient than the surrounding areas (Woodhouse, 2006) and this type of scattering is the key to understanding the performance of the developed salinity models.

The polarimetric decomposition techniques using scattering matrix are applied to understand the scattering mechanisms occurring at the resolution cell (Akhavan et al., 2021; Muhetaer et al., 2022). These techniques describe the scattering mechanisms very well in the case of a single dominant scatterer within the resolution cell where this scatterer changes the polarization of the incidence wave but faces serious challenges to describe the scattering mechanisms in the case of distributed scatterers within the resolution cells where these scatterers depolarized the incidence wave (Moreira et al., 2013). For this reason, the polarimetric decomposition parameters (Entropy, Anisotropy, Alpha) were calculated due to their ability to better describe the scattering mechanisms of distributed scatterers (Wang et al., 2016).

Table 3 shows that there is no correlation between soil salinity and Gamm0VH which results in low model performance for Gamma0VH (0.01). This can be related due to the low sensitivity of the VH channel to Bragg and surface scattering surfaces. While the VV channel showed a better measure for salinity content but the correlation is medium and the model based on Gamma0VV showed weak performance (0.313). Entropy and Alpha angle showed a stronger correlation with the soil salinity but in an inverse relationship. This is clear in the case of high salinity content where Bragg scattering is dominant which results in low Entropy due to the homogeneity of the scattering and low Alpha angle. In this condition, the salinity models based on Entropy and Alpha angle performed better than the condition of medium to low salinity, 0.59 and 0.56 respectively. Anisotropy showed a strong correlation with the soil salinity in a direct relationship which showed the existence of a dominant secondary scattering which can be considered as surface scattering because of the low Alpha angle in the high salinity region. The model based on Anisotropy performed close to the previous models with an R-square of 0.57.

The correlation between the polarimetric decomposition parameters and the measured soil salinity showed complex cases. Entropy and soil salinity showed a strong negative relationship with a value of -0.71 which indicates that the higher the salinity the higher the probability for a dominant scattering mechanism to occur because a zero value of Entropy means that there is only one scattering mechanism. Higher values of Entropy mean more chances for complicated scattering mechanisms to occur which can explain why the model is degrading when estimating medium to low salinity based on Entropy. In the case of Anisotropy, the correlation with soil salinity showed a positive relationship with a value of 0.61 which indicates that the higher the salinity the higher the chance for a dominant one secondary scattering mechanism. The correlation between the anisotropy and the salinity can partially explain the miss described portion of the relationship between the entropy and the salinity by the correlation between the entropy and anisotropy which showed a very strong negative relationship with a value of -0.96. Since high values of entropy indicate depolarizing scatterers, this can be supported by the low values of the anisotropy which indicate the absence of a dominant secondary scattering mechanism. This showed that in the case of high entropy and low anisotropy, it is still challenging to fully describe the scattering mechanism.

The H-a decomposition classification showed a further explanation for the complexity of describing the scattering mechanism for the study area. This classification showed that only 15% of the samples were classified as Bragg surface scattering, while 55% of the samples were classified as Random Surface Scattering, and 30% of the samples were unable to be described by the polarimetric decomposition technique. The scattering mechanism for only 15% of the samples to be fully described is the main reason for the models' performance.

6. Conclusions

This research study attempts to use active radar remote sensing for mapping saline soils within arid and semi-arid environments. Previous studies utilizing earth observation data for mapping saline soils have heavily focused on the use of broad band passive remote sensing. The results showed significant lower accuracies for active remote sensing in mapping saline soils. Accuracies obtained from the polarimetric decomposition parameters of entropy and anisotropy showed mere 17% and 15%, respectively, when compared to field measurements. This investigation of soil salinity mapping using Sentinel-1 data showed some limitations and challenges. Utilizing the dual polarization to fully describe the scattering mechanism can be considered a major limitation of this investigation. The polarimetric decomposition of dual polarization can describe a primary scattering mechanism and only one secondary scattering mechanism, which means that the anisotropy is not highly valuable. Furthermore, another challenge of this investigation arises from the nature of the complicated scattering mechanism, as 85% of the field soils samples were either identified as random scattering or unable to be described from the polarimetric decomposition parameters. The solution to fully describe the scattering mechanism can be by utilizing full polarization and/or circular polarization to gain a deep understanding of the scattering occurring at the resolution cell. In addition, it can hypothesised, at this stage that depending primarily on EC measurements with no consideration to other soil dielectric properties, surface roughness and moisture content brings high levels of uncertainties to the relationship. This issue will be addressed in future studies.

7. References

Abuelgasim, A., Ammad, R., 2017. Mapping Sabkha Land Surfaces in the United Arab Emirates (UAE) using Landsat 8 Data, Principal Component Analysis and Soil Salinity Information, International Journal of Engineering and Manufacturing, Vol. 7, Iss. 4, (Jul 2017): 1. DOI: 10.5815/ijem.2017.04.01

Abuelgasim, A., Ammad, R., 2019. Mapping soil salinity in arid and semi-arid regions using Landsat 8 OLI satellite data. Remote Sensing Applications: Society and Environment. 13, 415-425. https://doi.org/10.1016/j.rsase.2018.12.010

Akhavan, Z., Hasanlou, M., Hosseini, M., and McNairn H., 2021. Decomposition-Based Soil Moisture Estimation Using UAVSAR Fully Polarimetric Images. agronomy. 11, 145. https://doi.org/10.3390/agronomy11010145

Barbouchi, M., Abdelfattah, R., Chokmani, K., Aissa, N.B., Lhissou, R., Harti, A.E., 2015. Soil Salinity Characterization Using Polarimetric InSAR Coherence: Case Studies in Tunisia and Morocco. IEEE Journal of Selected Topics in Applied Earth Observations and Remote Sensing. 8, 3823-3832. https://doi.org/10.1109/JSTARS.2014.2333535

Cloude, S.R., Pottier, E., 1996. A review of target decomposition theorems in radar polarimetry. IEEE Trans. Geosci. Remote Sens. 34, 498–518. https://doi.org/10.1109/36.485127.

Davis, E., Wang, C., Dow, K., 2019. Comparing Sentinel-2 MSI and Landsat 8 OLI in soil salinity detection: a case study of agricultural lands in coastal North Carolina. International Journal of Remote Sensing. 40, 6134-6153. https://doi.org/10.1080/01431161.2019.1587205.

Gao, Y.; Liu, X.; Hou, W.; Han, Y.; Wang, R.; Zhang, H. Characteristics of Saline Soil in Extremely Arid Regions: A Case Study Using GF-3 and ALOS-2 Quad-Pol SAR Data in Qinghai, China. Remote Sens. 2021, 13, 417. https://doi.org/10.3390/rs13030417.

Hoa, P.V., Giang, N.V., Binh, N.A., Hai, L.V., Pham, T.-D., Hasanlou, M., et al., 2019. Soil Salinity Mapping Using SAR Sentinel-1 Data and Advanced Machine Learning Algorithms: A Case Study at Ben Tre Province of the Mekong River Delta (Vietnam). Remote Sensing. 11. https://doi.org/10.3390/rs11020128.

Ivushkin, K.; Bartholomeus, H.; Bregt, A.K.; Pulatov, A.; Kempen, B.; de Sousa, L. Global mapping of soil salinity change. Remote Sens. Environ. 2019, 231, 12, https://doi.org/10.1016/j.rse.2019.111260

Jiang, H., Rusuli, Y., Amuti, T., He, Q., 2019. Quantitative assessment of soil salinity using multi-source remote sensing data based on the support vector machine and artificial neural network. International Journal of Remote Sensing. 40, 284-306. https://doi.org/10.1080/01431161.2018.1513180.

Kaplan, G., Gašparović,M., Alqasemi,A., Aldhaheri,n A., Abuelgasim, A., Ibrahim, M., Soil salinity prediction using Machine Learning and Sentinel – 2 Remote Sensing Data in Hyper – Arid areas, Physics and Chemistry of the Earth, Parts A/B/C, Volume 130, 2023, https://doi.org/10.1016/j.pce.2023.103400.

Kissell, De.E., L. Sonon, L., Soil Test Handbook for Georgia Univ. Georgia Coop (2008) (Ext. Special Bul. 62).

Ma, G., Ding, J., Han, L., Zhang, Z., Ran, S., Digital mapping of soil salinization based on Sentinel-1 and Sentinel-2 data combined with machine learning algorithms, Regional Sustainability, Volume 2, Issue 2, 2021, Pages 177-188, https://doi.org/10.1016/j.regsus.2021.06.001.

Moreira, A., Prats-Iraola, P., Younis, M., Krieger, G., Hajnsek, I., Papathanassiou, K.P., 2013. A tutorial on synthetic aperture radar. IEEE Geosci. Remote Sens. Mag. 1, 6–43. https://doi.org/10.1109/MGRS.2013.2248301.

Muhetaer, N., Nurmemet, I., Abulaiti, A., Xiao, S., Zhao, J., 2022. A Quantifying Approach to Soil Salinity Based on a Radar Feature Space Model Using ALOS PALSAR-2 Data. Remote Sens. 14. https://doi.org/10.3390/rs14020363

Nurmemet, I., Sagan, V., Ding, J.-L., Halik, Ü., Abliz, A., Yakup, Z., 2018. A WFS-SVM Model for Soil Salinity Mapping in Keriya Oasis, Northwestern China Using Polarimetric Decomposition and Fully PolSAR Data. Remote Sensing. 10. https://doi.org/10.3390/rs10040598.

Periasamy, S., Ravi, K.P., 2020. A novel approach to quantify soil salinity by simulating the dielectric loss of SAR in three-dimensional density space. Remote Sensing of Environment. 251, 112059. https://doi.org/10.1016/j.rse.2020.112059.

Scudiero, E., Skaggs, T.H., Corwin, D.L., 2015. Regional-scale soil salinity assessment using Landsat ETM+ canopy reflectance. Remote Sensing of Environment. 169, 335-343. https://doi.org/10.1016/j.rse.2015.08.026.

Seifi, M., Ahmadi, A., Neyshabouri, M.-R., Taghizadeh-Mehrjardi, R., Bahrami, H.-A., 2020. Remote and Vis-NIR spectra sensing potential for soil salinization estimation in the eastern coast of Urmia hyper saline lake, Iran. Remote Sensing Applications: Society and Environment. 20, 100398. https://doi.org/10.1016/j.rsase.2020.100398.

Taghadosi, M.M., Hasanlou, M., Eftekhari, K., 2019. Soil salinity mapping using dual-polarized SAR Sentinel-1 imagery. International Journal of Remote Sensing. 40, 237-252. https://doi.org/10.1080/01431161.2018.1512767.

Wang, J., Peng, J., Li, H., Yin, C., Liu, W., Wang, T., Zhang, H., 2021. Soil salinity mapping using machine learning algorithms with the sentinel-2 MSI in arid areas, China. Remote Sens. 13, 1–14. https://doi.org/10.3390/rs13020305.

Woodhouse, I.H., 2006. Introduction to microwave remote sensing. CRC Press, Taylor & Francis, Boca Raton, Florida.

Yahiaoui, I., Bradaï, A., Douaoui, A., Abdennour, M.A., 2021. Performance of random forest and buffer analysis of Sentinel-2 data for modelling soil salinity in the Lower-Cheliff plain (Algeria). International Journal of Remote Sensing. 42, 148-171. https://doi.org/10.1080/0143116

Smith, J., 1987b. Economic printing of color orthophotos. Report KRL-01234, Kennedy Research Laboratories, Arlington, VA, USA.

Smith, J., 2000. Remote sensing to predict volcano outbursts. *Int. Arch. Photogramm. Remote Sens. Spatial Inf. Sci.*, XXVII-B1, 456-469.